Pinpointing the neural signatures of single-exposure visual familiarity

Vahid Mehrpour[1], Travis Meyer[1], Eero P. Simoncelli[2] and Nicole C. Rust[1*]

[1]Department of Psychology, University of Pennsylvania
[2]Howard Hughes Medical Institute and Center for Neural Science, New York University

* Correspondence to: nrust@psych.upenn.edu

Abstract: Memories of the images that we have seen are thought to be reflected in the reduction of neural responses in high-level visual areas such as inferotemporal (IT) cortex, a phenomenon known as repetition suppression (RS). We challenged this hypothesis with a task that required rhesus monkeys to report image familiarity while ignoring variations in contrast, a stimulus attribute that is also known to modulate the overall IT response. The monkeys' behavior was largely contrast-invariant, contrary to the predictions of the RS encoding scheme, which could not distinguish response familiarity from changes in contrast. However, the monkeys' behavioral patterns were well predicted by a linearly decodable variant in which the total spike count is corrected for contrast modulation. These results suggest that the IT neural activity pattern that best aligns with single-exposure visual familiarity behavior is not RS but rather "sensory referenced suppression (SRS)": reductions in IT population response magnitude, corrected for sensory modulation.

Introduction:

Under the right conditions, we are very good at remembering the images that we have seen: we can remember thousands of images after viewing each only once and only for a few seconds [1, 2]. How our brains support this remarkable ability is not well understood. The most prominent proposal to date suggests that visual familiarity is signaled in high-level visual brain areas such as inferotemporal cortex (IT) and perirhinal cortex via adaptation-like reductions of the population response to familiar as compared to novel stimuli, a phenomenon referred to as *repetition suppression* (RS) [3-8]. Repetition suppression exhibits the primary attributes needed to account for the vast capacity of single-exposure visual memory behavior: response decrements in subsequent exposures are selective for image identity (even after viewing an extensive sequence of other images), and last for several minutes to hours [4, 5, 9]. RS has also been shown to account for behavior in an image familiarity task: a linear decoder with positive weights can predict single-exposure visual memory behavior from neural responses in IT cortex [9].

Despite the fact that the RS hypothesis is consistent with available evidence, it seems likely to be too simplistic an explanation for visual memory encoding. In particular, it is well-known that sensory neurons such as those of IT cortex are modulated not only by visual familiarity, but also by stimulus properties such as image contrast [10]. It is thus unclear whether and how these stimulus-induced effects interfere with judgments of familiarity, and if they do not, how familiarity can be decoded from neural responses in a way that disambiguates it from changes in these stimulus properties. To investigate this, we measured behavioral and neural responses of monkeys trained to report whether images were novel or familiar while disregarding image contrast (Fig 1a).

Results:

The contrast-invariant visual memory task:

Monkeys viewed sequences of grayscale images, each presented for 500 ms, and each presented exactly twice (initially novel, then familiar). Novel and familiar images were presented with equal probability in all possible combinations of high (H) and low (L) contrasts, including (novel, familiar): HH, LL, HL, LH. We refer to the former two cases as the “same-contrast” conditions and the latter two as the “mixed-contrast” conditions (Fig 1b). Monkeys were trained to report, on each trial, whether the observed image was novel or familiar, while disregarding image contrast (Fig 1a). After training, the monkeys were largely able to disambiguate changes in familiarity from changes in image contrast: they performed equally well for both same-contrast conditions, and they were only modestly impaired for the mixed-contrast conditions (Fig 1c). We quantified the degree of contrast invariance in the behavioral patterns with a measure in the range 0-1, where 1 indicates a behavioral pattern that is perfectly contrast invariant and 0 corresponds to the pattern that is maximally contrast dependent after taking into account the monkeys’ overall performance in each memory condition (see Fig 1c

insets). Behavioral contrast invariance values were high (combined data: 0.87; monkey1: 0.95, monkey2: 0.84; Supp Fig 1), indicating that the monkeys were able to judge image familiarity while largely disregarding image contrast.

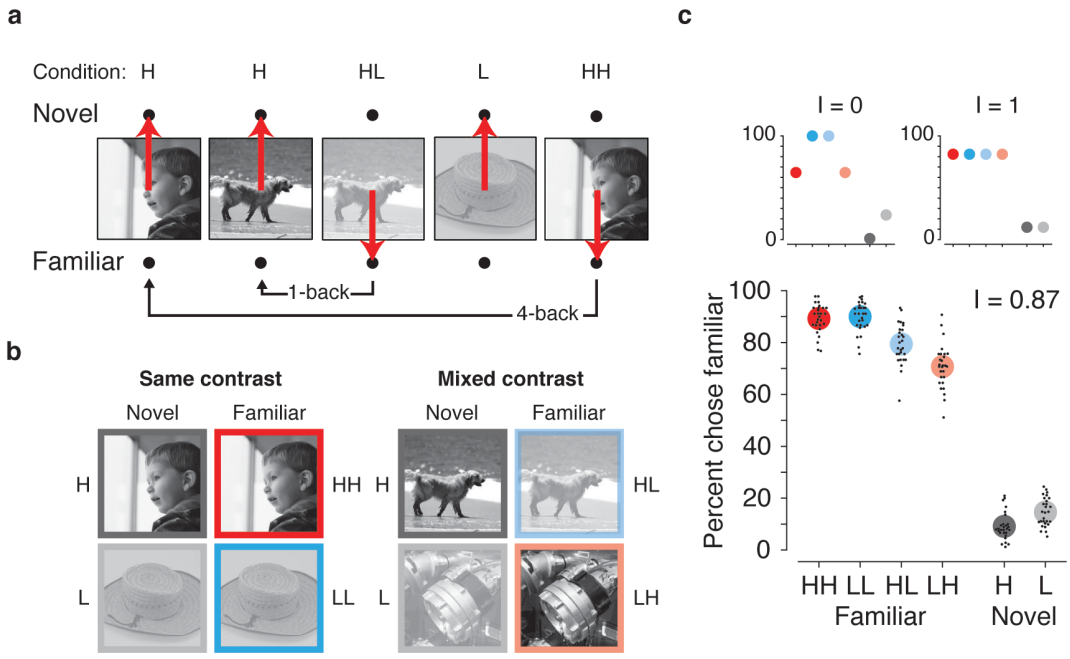

Figure 1. *Visual memory behavior.* **(a)** The contrast-invariant, single-exposure visual memory task. The monkeys viewed a sequence of images and reported whether they were novel (never seen before) or familiar (seen exactly once) while ignoring randomized changes in contrast. Monkeys were trained to saccade to one of two response targets to indicate their choice (red arrows). Images were repeated with a randomly chosen delay between the first and repeated presentation ('n-back'). **(b)** Images were displayed at one of two contrast levels, yielding two conditions for novel images, high (H) and low (L), and four conditions for familiar images: HH (familiar H preceded by novel H), LL (familiar L preceded by novel L), HL (familiar L preceded by novel H), LH (familiar H preceded by novel L). The four familiar conditions were organized into "same-contrast" and "mixed-contrast" groups depending on whether the initial and repeated presentations were at the same or different contrasts, respectively. **(c)** Behavioral performance for the data pooled across monkeys in the task, where small black dots indicate average performance for an individual session and large colored dots indicate the average performance across sessions. A measure of contrast invariance, I, was computed as the ratio of the variance across contrast conditions and the variance with respect to the maximally contrast modulated pattern after taking overall performance into account, subtracted from one (see Methods). Insets illustrate the expected behavioral pattern with minimal (I = 0) and maximal (I = 1) contrast invariance.

RS and optimally weighted linear decoders fail to predict behavior:

As the monkeys performed the task, we recorded neural responses in IT. Because accurate estimates of population response magnitude require many hundreds of units, data were concatenated across sessions into a larger pseudopopulation in a manner that combined trials within the same experimental condition (see Methods). Spikes were counted in a window starting 100 ms after stimulus onset (to allow for the latency of visual signals arriving in IT) and ending 400 ms later, at the termination of the image

viewing period. The resulting pseudopopulation contained the responses of 856 units to 180 images each presented twice, and distributed evenly (and randomly) within the four conditions (i.e. 45 images for each of HH, LH, HL, LL).

We began by assessing the hypothesis that RS of IT responses can explain visual memory behavior. We instantiated this hypothesis with a total spike count decoder, in which familiarity was determined by comparing the total spike count with a threshold. The quality of the alignment between neural predictions of behavioral patterns and the monkeys' actual behavior, termed 'prediction quality (PQ)', benchmarks the MSE between the actual behavioral patterns and neural predictions of behavior between the worst-possible and best-possible scenarios (see Methods). The upper bound of our measure, PQ = 1, reflects a neural prediction that perfectly replicates the actual behavioral pattern. A PQ = 0 reflects the worst possible predicted behavioral pattern that was matched in overall performance (e.g., a pattern that was modulated entirely by changes in contrast, analogous to the insets in Fig 1c). This 'RS' decoder confounded changes in familiarity with changes in contrast and produced a poor behavioral prediction (PQ_{RS} = 0.40; Fig 2a).

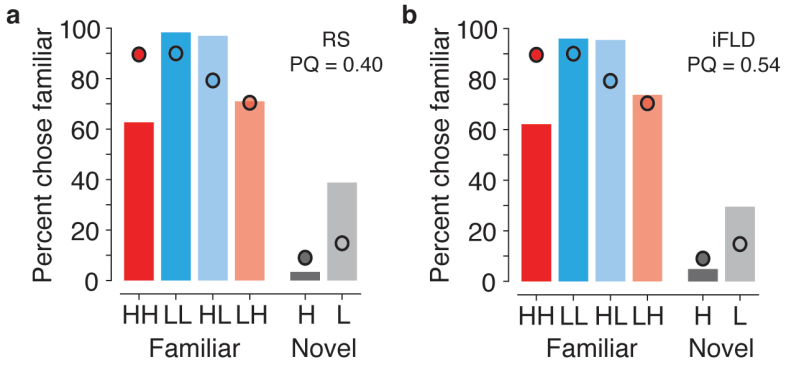

Figure 2. *Traditional linear decoders confuse familiarity and contrast and fail to map IT neural responses to behavior.* Each panel reflects the monkeys' actual behavioral patterns (dots) along with the predictions of a linear decoder applied to the recorded neural population (bars). (**a**) Total spike count decoder, motivated by RS. **(b)** Optimally weighted linear decoder, iFLD. Prediction quality (PQ) quantifies similarity between the neural predictions of behavior and the monkeys' actual behavioral patterns (see Text).

The RS decoder is a linear decoder with uniform weighting over the neural population, so we wondered whether more carefully chosen weights might yield a linear decoder that could match the behavioral responses. Specifically, an optimally-weighted linear decoder was previously shown to be effective at aligning IT neural responses with visual memory behavior in the absence of contrast modulation [9]. We used this same Fisher Linear Discriminant, computed assuming independence of neural responses, that weights each unit proportional to its discriminability, d' (iFLD; see Methods). The iFLD differs from RS in that it weights each unit according to the amount of task-relevant information that it carries, and these weightings are signed: should any units that exhibit

repetition enhancement (on average) exist, those would be appropriately combined with opposite sign with units that exhibit repetition suppression. Despite the fact that this decoder is optimized to extract familiarity information while disregarding contrast, we found that the iFLD also confused changes in familiarity with changes in contrast, and behavioral predictions were only slightly improved relative to RS (PQ_{iFLD} = 0.54; Fig 2b). Poor behavioral predictions for RS and iFLD were replicated for each monkey individually (Supp. Fig 2; monkey 1: PQ_{RS} = 0.61, PQ_{iFLD} = 0.66; monkey 2: PQ_{RS} = 0.19, and PQ_{iFLD} = 0.53). We return to examine the underlying reasons for this failure below, in Figure 5.

Sensory referenced suppression is a good predictor of behavior:

We wondered whether the monkeys' behavioral patterns could be explained by any linear decoder applied to the IT population. Given the substantial evidence in support of the repetition suppression hypothesis, we reasoned that the brain might be acting on a variant of this neural signature in which it corrects for the ambiguities in total spike count that are introduced by changes in contrast. Because this hypothetical decoding scheme operates by estimating and correcting for modulations in the total spike count due to variations in memory-irrelevant sensory attributes, we refer to this hypothesis as "sensory referenced suppression (SRS)".

What would be required for SRS to be an effective account of the mapping of IT neural signals to behavior, if such a decoding scheme were restricted to act only on the IT population response? Minimally, information about contrast would have to be reflected along a linear axis in IT that is at least partially non-overlapping with the total spike count. We found that this was indeed the case: an optimized decoding vector for contrast lies in a direction 69 degrees from the total spike count vector (labeled RS), indicating that information about contrast was largely non-overlapping but not quite orthogonal to RS (Fig 3a). Consider the family of linear discrimination vectors that live on the 2-D plane defined by RS and the contrast decoder. On this plane, we define angles of 0 degrees as the total spike count RS decoder with no contrast correction (see Fig 3a, top inset: 'RS'). Vectors on this plane that are rotated in the clockwise direction (i.e. negative angles) can be interpreted as linear decoders that estimate and correct the total spike count for contrast, implemented as a weighted linear combination of the RS and contrast decoders to produce a new linear decoder. In comparison, positive angles exacerbate contrast modulation in the predicted behavioral patterns. Within this family of linear decoding schemes, we defined SRS as the decoder that was orthogonal to (i.e. 90 ^{o} from) the contrast decoder, and consequently minimized contrast modulation in the neural prediction of behavioral patterns. The SRS was -21^{o} from RS for the data pooled across both monkeys (Fig 3b) and -23^{o} and -18^{o} for individual animals (Supp Fig 3).

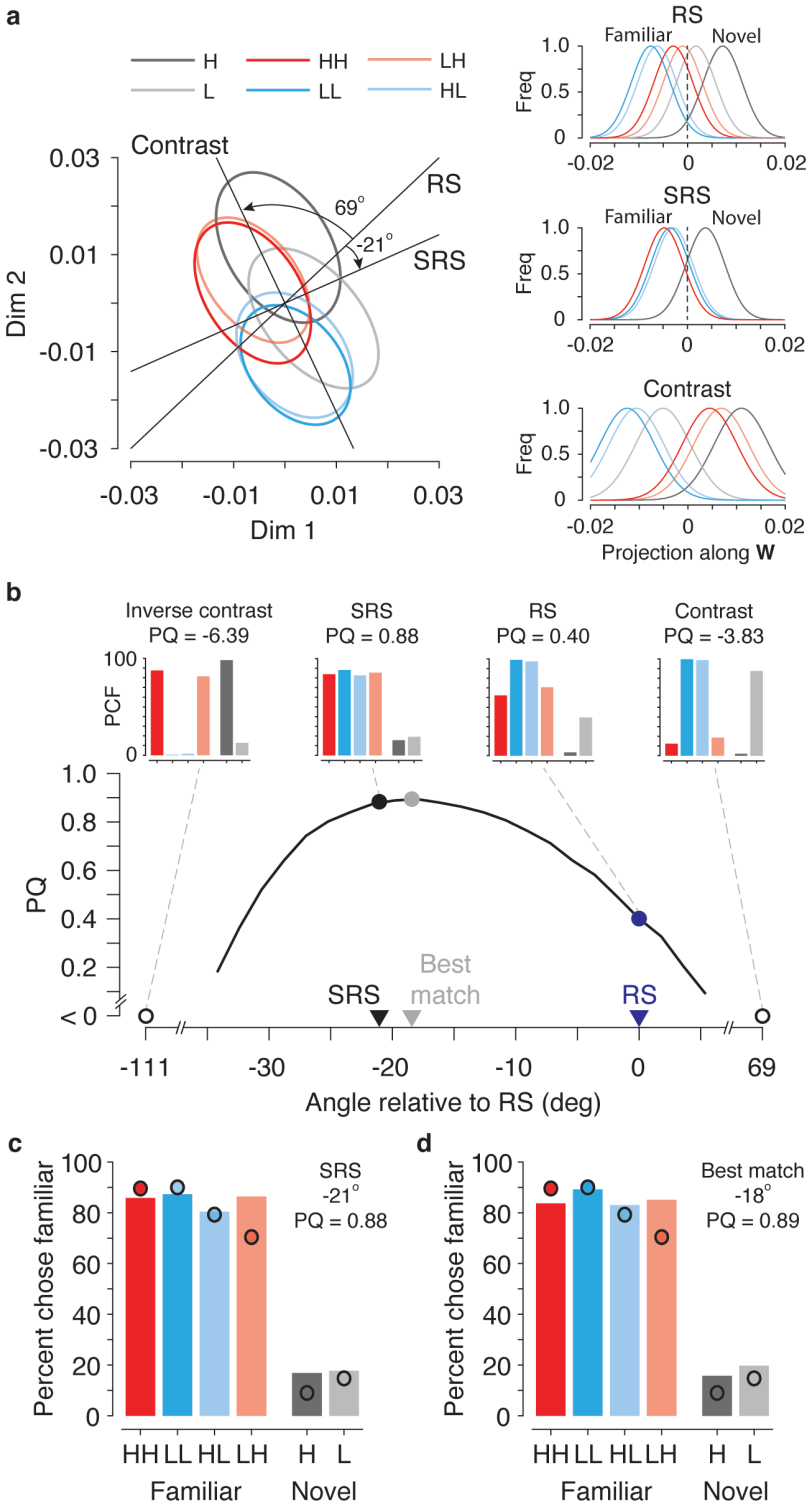

Figure 3. *Neural predictions of behavior for a family of weighted linear decoders that include RS, an optimized contrast decoder, and SRS.* (**a**) Projections of IT neural response distributions for all 6 stimulus conditions onto the 2-D plane defined by weight vectors for the total spike count vector ('RS', which uses a weight vector of all ones) and for a linear decoder optimized for contrast ('Contrast'). Ellipses depict 95% confidence intervals for 2-D histograms of the projection of neural responses onto this plane (see Methods). Insets show 1-D histograms of the projections of the distributions onto the three linear decoders. (**b**) The quality of the neural predictions of monkeys' behavioral patterns (PQ) for the family of linear decoders that lie within the plane. Negative PQ values reflect predicted behavioral patterns that could not be rescaled to match overall performance because one or more entries were pinned at saturation (e.g., as a consequence of extreme contrast modulation). Each decoder corresponds to a rotation of the total spike count decoder, or equivalently, the weighted combination of the total spike count decoder and the contrast decoder. Markers indicate: SRS (black), which has minimal contrast sensitivity (i.e., orthogonal to the contrast axis); RS (blue), the total spike count decoder with no contrast correction; and the best behavioral match (maximal PQ – gray). Insets above depict the corresponding neural predictions of behavior. (**c-d**) The alignment of the monkeys' actual behavioral patterns (dots) and the neural predictions of behavior (bars) for (**c**) SRS and (**d**) the decoder with the best behavioral match.

The SRS linear decoder did a very good job at predicting the monkeys' behavioral patterns, both for the pooled data (PQ_{SRS} = 0.88; Fig 3c), and for each monkey individually (monkey 1: PQ_{SRS} = 0.87; monkey 2: PQ_{SRS} = 0.93; Supp Fig 3). It also provided a much better prediction of behavior than RS or the iFLD (pooled data: PQ_{RS} = 0.40 & PQ_{iFLD} = 0.54; monkey 1: PQ_{RS} = 0.61 & PQ_{iFLD} = 0.66; monkey 2: PQ_{RS} = 0.19 & PQ_{iFLD} = 0.53). These results suggest that SRS provides a considerably better description of the relationship between IT neural activity and behavior than RS or iFLD under the challenge of sensory variation in population response magnitude (i.e. contrast modulation). Additionally, these results reveal that the sensory information required to perform the correction for contrast is linearly decodable from IT itself.

The SRS decoder had better familiarity performance than RS:

To better understand how memory and contrast were reflected in IT during these experiments, we shifted our focus away from the alignment between decoding predictions and behavior and toward overall performance in decoding familiarity. These issues are best conceptualized by considering discriminability (d'), rather than percent correct, as a measure of performance computed as the ratio of the difference between the means of the novel and familiar distributions divided by the square root of the average variance for those distributions (Fig 4a). In our experiments, the variance of each distribution can be further decomposed into two components: (1) modulations within each distribution by contrast (Fig 4a, 'Contrast Var'), and (2) combined modulations arising from image identity and trial variability (which cannot be dissociated, due to the single-trial nature of these experiments; Fig 4a, 'ID Var').

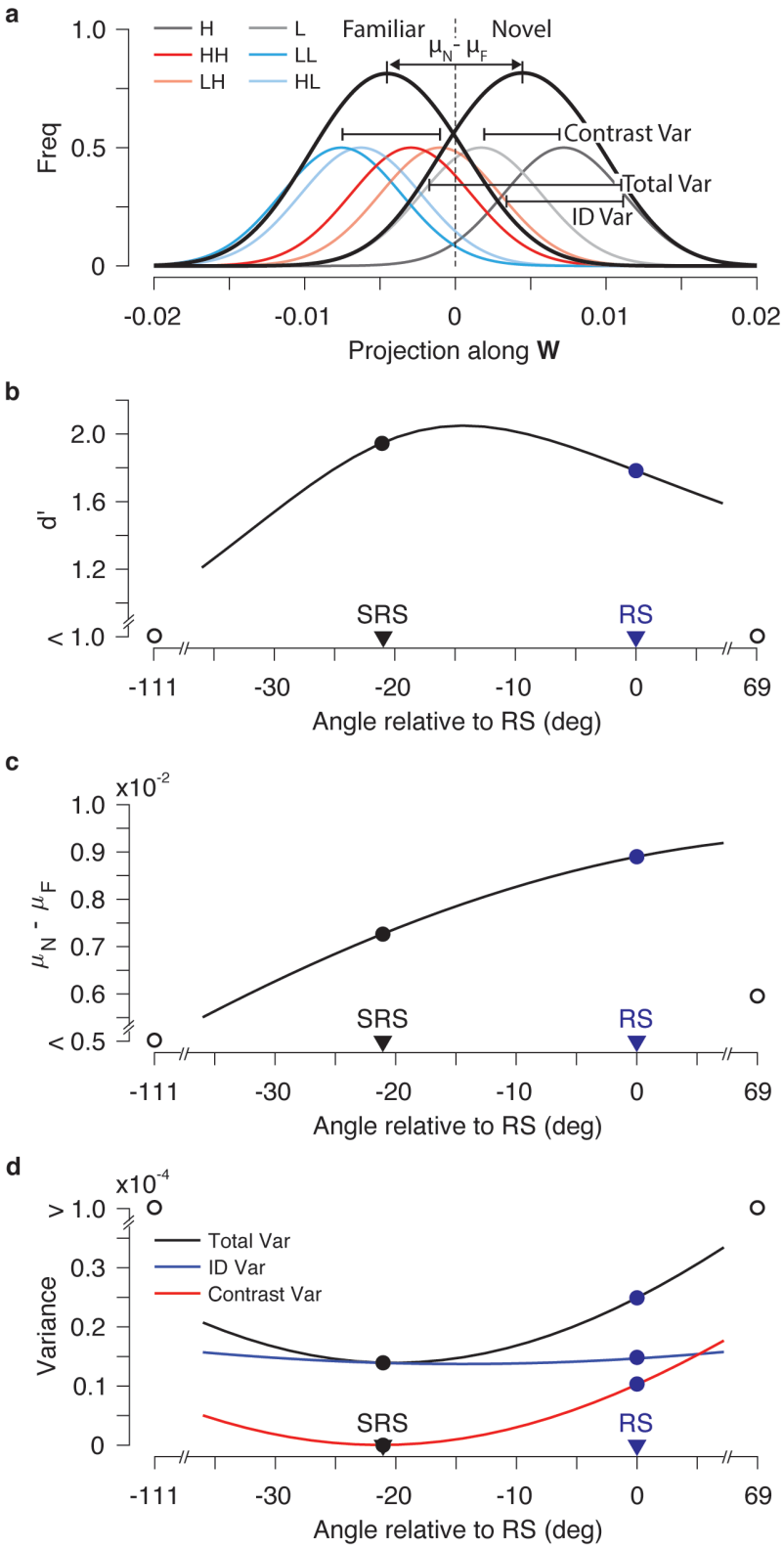

Figure 4. *The population geometry impacting overall familiarity performance for SRS and RS.* (**a**) A schematic of linear decoder performance, computed as d', for this task. Shown are 1-D histograms of the

projection of the IT population responses onto a linear decoding axis **W.** Discriminability for familiarity (d') is computed as the difference between the means of novel and familiar distributions ($\mu_N - \mu_F$) divided by the square root of the average total variance (total Var). (**b**) d' as a function of angle on the 2-D plane defined in Fig 3a. (**c-d**) Decomposition of d': **(c)** the numerator (difference between means), and (**d**) the square of the denominator, the total variance (Total Var), further broken down into the variance due to image identity and trial variability (ID Var) and contrast modulation (Contrast Var) – see Methods. In b-d, open circles at the right side of each graph indicate the values for projections along the contrast decoder.

We found that, in addition to being a better predictor of behavior (Fig 3b), the SRS decoder also had higher familiarity performance than RS (Fig 4b). This occurred despite the fact that novel and familiar means were actually closer together along the SRS direction than the RS direction (Fig 4c). These decreases in mean separation were offset by even larger decreases in variance (denominator of d'), plotted in Fig 4d. These decreases in variance could in turn be attributed entirely to the elimination of contrast modulation. In sum, the superior performance of SRS resulted from novel and familiar distributions whose means were slightly closer together, but whose variances decreased even more as a consequence of eliminating contrast modulation along the SRS linear decoding axis.

Relationship between SRS and iFLD decoders:

The results presented above demonstrate that while the largely contrast-invariant patterns reflected in monkeys' behavior are linearly decodable from IT neural responses with the SRS decoder (Fig 3c), a linear decoder optimized for familiarity on our data (the iFLD) confuses changes in familiarity with changes in contrast (Fig 2b). What do these differences imply about the geometry by which familiarity and contrast are reflected in IT? To address these questions, we turned to simulations, where issues about population geometry can be investigated absent the constraints imposed by finite samples. To perform these simulations, we began by fitting a model to each single unit that we recorded. For each IT unit, the distribution of the visually-evoked firing rate response over stimuli was modeled as an exponential [11], familiarity and contrast were modeled as multiplicative modulations of the visually-evoked response, and trial-to-trial variability in spike counts was modeled as an independent Poisson process (see Methods). The four parameters fit for each unit included: (1) mean firing rate (the mean of the exponential), (2) the visually-evoked tuning bandwidth, (3) familiarity sensitivity, and (4) contrast sensitivity (see Methods). We found that 'synthetic' data from the resulting model population recapitulated all aspects of the physiological data that we have highlighted thus far, including contrast modulation in the RS predictions (Supp Fig 4a, top inset), contrast-invariant SRS (Supp Fig 4a, middle inset), and overall d' that was higher for SRS than RS as a consequence of eliminating contrast modulation (Supp Fig 4b-d).

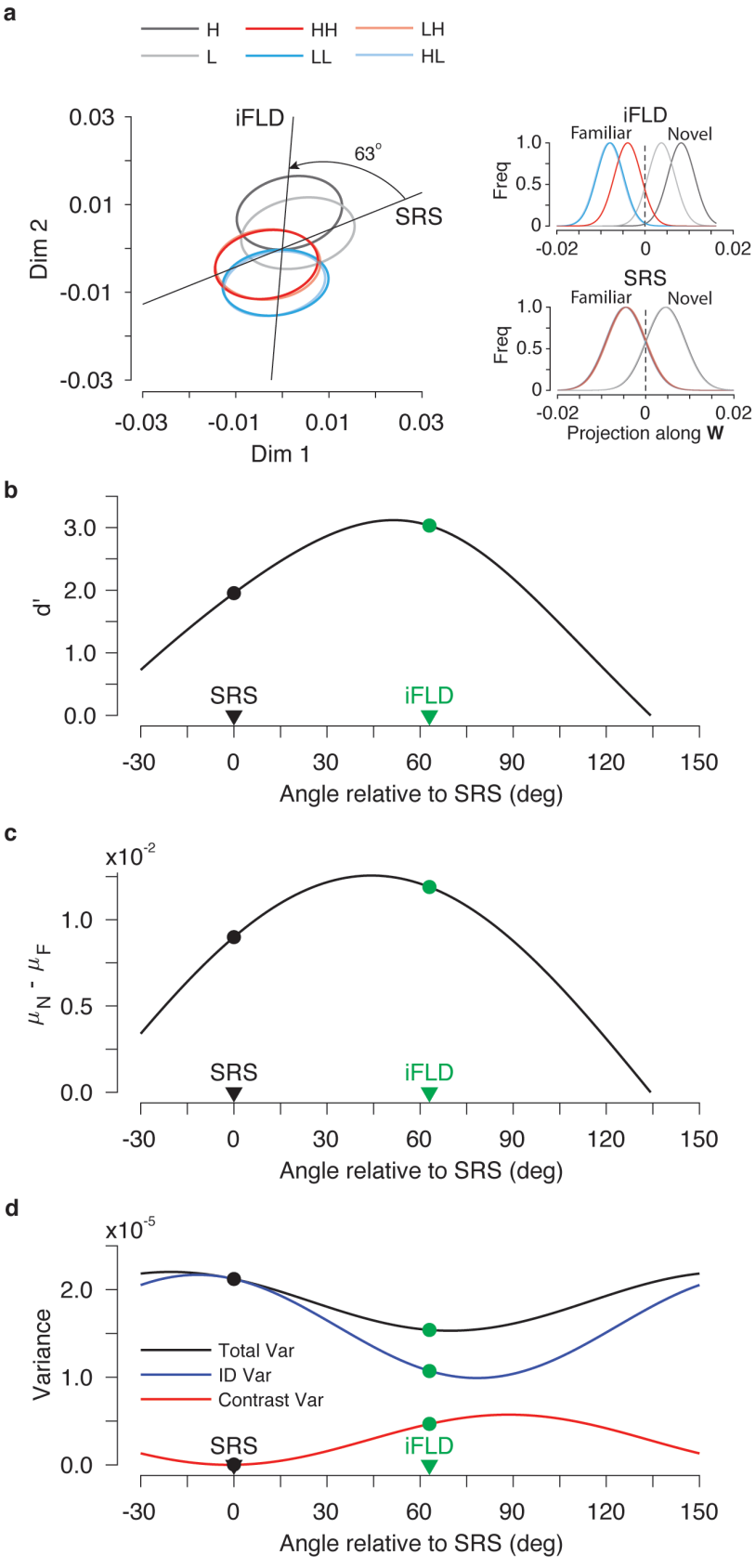

Figure 5. *The population geometry impacting overall performance for SRS and iFLD.* To explore population geometry absent the constraints imposed by limited samples, a model was fit to each unit and model parameters were used to create synthetic data. **(a)** Projections of the synthetic data onto the 2-D plane defined by SRS and a linear decoder optimized for memory, 'iFLD'. Ellipses depict 95% confidence intervals for 2-D histograms of the projection of neural responses onto this plane. Insets show 1-D histograms of the projections onto each linear axis. **(b)** d' as a function of angle relative to SRS on the 2-D plane defined in panel a. **(c-d)** Decomposition of d' into **(c)** It's numerator, the difference between the means of the novel and familiar distributions and **(d)** The square of its denominator, the total variance (Total Var), further broken down into the variance due to image identity and trial variability (ID Var) and contrast modulation (Contrast Var). In b-d, values corresponding to SRS and iFLD are labeled by black and green markers, respectively.

Next, to understand the relationship between SRS and the iFLD, and why the iFLD did not exhibit contrast invariance, we performed a set of analysis similar to those described for Figure 3-4 but within the plane spanned by SRS and iFLD (Fig 5a). The iFLD is optimal (under the assumption of Gaussian-distributed independent response), and indeed has higher discrimination performance than SRS (Fig 5b). Increased d' for iFLD over SRS resulted from both an increase in the distance between the means of the novel and familiar distributions (i.e. the d' numerator; Fig 5c) as well as a decrease in the variance between the novel and familiar distributions (i.e. the d' denominator; Fig 5d). Intriguingly, the overall reduction in total variance along the iFLD axis relative to SRS resulted from *increases* in contrast modulation that were offset by a larger decreases in identity modulation relative to SRS (Fig 5d). This was because identity modulations and contrast modulations were anti-correlated on this plane: decreases in one (e.g. identity modulation) were accompanied by increases in the other (e.g. contrast modulation; Fig 5d). In other words, the iFLD failed to predict contrast invariance in behavioral patterns because it could achieve higher familiarity performance by reducing identity variance, which is anti-correlated with contrast.

Discussion

Understanding the neural mechanisms that support the remarkable ability that humans and nonhuman primates have to remember the images that they have seen[1, 2, 4, 5, 12] requires pinpointing the neural activity patterns that reflect visual familiarity behavior. Here we challenged suggestions that visual familiarity is signaled in high-level visual brain areas such as IT via changes in population response magnitude, or repetition suppression (RS) [3-8], by manipulating another factor known to modulate IT neural responses, image contrast. The monkeys were largely able to report visual familiarity invariant to changes in image contrast (Fig 1) whereas the IT population response was modulated by contrast and consequently, behavioral invariance could not be reconciled with RS (Fig 2a). Behavioral invariance also could not be reconciled with our previous work suggesting that familiarity could be decoded from IT with an optimized linear decoding scheme that weights each neuron proportional to its d', or equivalently, the amount and sign of the task-relevant information that it carries [9] (Fig 2b). However, the

monkeys' behavioral patterns were linearly decodable from IT (Fig 3c), using a linear decoder that corrects the total spike count decoder by eliminating its contrast dependence. We call this linear decoding scheme sensory referenced suppression 'SRS', because it can be understood as estimating familiarity from the total spike count after correcting for sensory modulation (Fig 3a).

The hypothesis that visual familiarity is encoded in high-level visual cortex as RS has a mixed history, with some studies finding support for this hypothesis[5, 7, 9, 13, 14] and others finding evidence against it[15, 16]. Our work suggests that modifications of RS are required to account for single-exposure visual memory behavior when factors other than familiarity modulate the magnitude of the population response. A number of factors other than contrast are known to modulate the IT population response in this way, including stimulus attributes such as object size[10], and a diverse set of stimulus attributes that contribute to image memorability[17-19], as well as external factors such as surprise[20, 21] and attention[7, 22]. The SRS decoding scheme that we have proposed could, in principle, provide a mechanism for the brain to disambiguate familiarity-induced changes in IT population response magnitude from changes due to the combination of all of these other factors. Similarly, our results inform a broader understanding of how the brain might disambiguate any one of these magnitude-coded variables from the rest: for example, detecting when something surprising has happened across fluctuations in other variables.

What is the origin of the IT magnitude variation that aligns with single-exposure familiarity-based behavior? It is likely to be the combined product of multiple sources. RS is found at all stages of visual processing from the retina to IT, and it strengthens in its magnitude as well as the duration over which it lasts as one ascends the visual cortical hierarchy [23]. Consequently, a hierarchical cascade of feed-forward, adaptation-like mechanisms may underlie RS measured in IT [24]. There are also indications that RS within IT may arise from changes in synaptic weights between recurrently connected units within IT itself [24, 25]. Finally, a component of RS in IT is likely to be fed back from higher brain areas such as perirhinal cortex or hippocampus. While the assertion that top-down processing contributes to RS in high-level visual cortex has been controversial [24, 26-28], recent evidence from a patient with medial temporal lobe (MTL) damage supports a role for feedback from MTL structures to RS in high-level visual cortex[29]. Within the one MTL structure, the hippocampus, single-exposure familiarity behavior has been linked with repetition suppression [30, 31] as well as synchronizations between gamma oscillations and spikes [32]. Because these evaluations were not been made in a manner that challenges RS with other factors that affect response magnitude, additional work will be required to determine whether SRS is a better description than RS of the neural signatures that reflect single-exposure visual familiarity behavior in MTL structures.

Acknowledgments

This work was supported by the Simons Foundation (Simons Collaboration on the Global Brain award 543033 to NCR and 543047 to EPS), the National Eye Institute of the National Institutes of Health (award R01EY020851 to NCR), the National Science Foundation (CAREER award 1265480 NCR), and the Howard Hughes Medical Institute (investigatorship to EPS).

REFERENCES

Citation Diversity Statement

Recent work in neuroscience and related fields has identified citation biases whereby work from women and minorities are under-cited relative to other papers in the field[33-35]. In crafting this manuscript, we sought to proactively consider citation bias. Following ref. [33], the gender balance of citations was quantified based on the first names of the first and last authors using open source code[36]. Excluding self-citations, the references for this manuscript contain 59% man/man, 17% man/woman, 21% woman/man, and 3% woman/woman citations. Expected proportions estimated from 5 top neuroscience journals (as reported in ref. [33]) are 58.4% man/man, 9.4% man/woman, 25.5% woman/man, and 6.7% woman/woman.

1. Standing, L. Learning 10,000 pictures. *Q. J. Exp. Psychol.* **25**, 207-222 (1973).
2. Brady, T.F., Konkle, T., Alvarez, G.A. & Oliva, A. Visual long-term memory has a massive storage capacity for object details. *Proceedings of the National Academy of Sciences* **105**, 14325-14329 (2008).
3. Fahy, F.L., Riches, I.P. & Brown, M.W. Neuronal activity related to visual recognition memory: long-term memory and the encoding of recency and familiarity information in the primate anterior and medial inferior temporal and rhinal cortex. *Experimental Brain Research* **96**, 457-472 (1993).
4. Li, L., Miller, E.K. & Desimone, R. The representation of stimulus familiarity in anterior inferior temporal cortex. *Journal of Neurophysiology* **69**, 1918-1929 (1993).
5. Xiang, J.Z. & Brown, M.W. Differential neuronal encoding of novelty, familiarity and recency in regions of the anterior temporal lobe. *Neuropharmacology* **37**, 657-676 (1998).
6. Desimone, R. Neural mechanisms for visual memory and their role in attention. *Proceedings of the National Academy of Sciences* **93**, 13494-13499 (1996).
7. Miller, E.K., Li, L. & Desimone, R. A neural mechanism for working and recognition memory in inferior temporal cortex. *Science* **254**, 1377-1379 (1991).
8. Riches, I.P., Wilson, F.A. & Brown, M.W. The effects of visual stimulation and memory on neurons of the hippocampal formation and the neighboring parahippocampal gyrus and inferior temporal cortex of the primate. *J Neurosci* **11**, 1763-1779 (1991).
9. Meyer, T. & Rust, N.C. Single-exposure visual memory judgments are reflected in inferotemporal cortex. *eLife* **7**, e32259 (2018).
10. Zoccolan, D., Kouh, M., Poggio, T. & DiCarlo, J.J. Trade-off between object selectivity and tolerance in monkey inferotemporal cortex. *J Neurosci* **27**, 12292-12307 (2007).
11. Rust, N.C. & DiCarlo, J.J. Balanced increases in selectivity and tolerance produce constant sparseness along the ventral visual stream. *J Neurosci* **32**, 10170-10182 (2012).
12. Ringo, J.L. & Doty, R.W. A macaque remembers pictures briefly viewed six months earlier. *Behavioural brain research* **18**, 289-294 (1985).
13. Gonsalves, B.D., Kahn, I., Curran, T., Norman, K.A. & Wagner, A.D. Memory strength and repetition suppression: multimodal imaging of medial temporal cortical contributions to recognition. *Neuron* **47**, 751-761 (2005).

14. Turk-Browne, N.B., Yi, D.J. & Chun, M.M. Linking implicit and explicit memory: common encoding factors and shared representations. *Neuron* **49**, 917-927 (2006).
15. Ward, E.J., Chun, M.M. & Kuhl, B.A. Repetition suppression and multi-voxel pattern similarity differentially track implicit and explicit visual memory. *J Neurosci* **33**, 14749-14757 (2013).
16. Xue, G. *et al.* Spaced learning enhances subsequent recognition memory by reducing neural repetition suppression. *J Cogn Neurosci* **23**, 1624-1633 (2011).
17. Jaegle, A. *et al.* Population response magnitude variation in inferotemporal cortex predicts image memorability. *Elife* **8** (2019).
18. Isola, P., Jianxiong, X., Parikh, D., Torralba, A. & Oliva, A. What Makes a Photograph Memorable? *IEEE Trans Pattern Anal Mach Intell* **36**, 1469-1482 (2014).
19. Bainbridge, W.A., Isola, P. & Oliva, A. The intrinsic memorability of face photographs. *J Exp Psychol Gen* **142**, 1323-1334 (2013).
20. Meyer, T. & Olson, C.R. Statistical learning of visual transitions in monkey inferotemporal cortex. *Proc Natl Acad Sci U S A* **108**, 19401-19406 (2011).
21. Schwiedrzik, C.M. & Freiwald, W.A. High-Level Prediction Signals in a Low-Level Area of the Macaque Face-Processing Hierarchy. *Neuron* **96**, 89-97 e84 (2017).
22. Roth, N. & Rust, N.C. Inferotemporal cortex multiplexes behaviorally-relevant target match signals and visual representations in a manner that minimizes their interference. *PLoS One* **13**, e0200528 (2018).
23. Zhou, J., Benson, N.C., Kay, K.N. & Winawer, J. Compressive temporal summation in human visual cortex. *J. Neurosci.* **38**, 691-709 (2018).
24. Vogels, R. Sources of adaptation of inferior temporal cortical responses. *Cortex* **80**, 185-195 (2016).
25. Lim, S. *et al.* Inferring learning rules from distributions of firing rates in cortical neurons. *Nat. Neurosci.* **18**, 1804-1810 (2015).
26. Summerfield, C., Trittschuh, E.H., Monti, J.M., Mesulam, M.M. & Egner, T. Neural repetition suppression reflects fulfilled perceptual expectations. *Nat Neurosci* **11**, 1004-1006 (2008).
27. Grotheer, M. & Kovacs, G. Repetition probability effects depend on prior experiences. *J Neurosci* **34**, 6640-6646 (2014).
28. Vinken, K., Op de Beeck, H.P. & Vogels, R. Face Repetition Probability Does Not Affect Repetition Suppression in Macaque Inferotemporal Cortex. *J Neurosci* **38**, 7492-7504 (2018).
29. Kim, J.G. *et al.* Functions of ventral visual cortex after bilateral medial temporal lobe damage. *Prog Neurobiol* **191**, 101819 (2020).
30. Sakon, J.J. & Suzuki, W.A. A neural signature of pattern separation in the monkey hippocampus. *Proc Natl Acad Sci U S A* **116**, 9634-9643 (2019).
31. Suthana, N.A. *et al.* Specific responses of human hippocampal neurons are associated with better memory. *Proc Natl Acad Sci U S A* **112**, 10503-10508 (2015).
32. Jutras, M.J., Fries, P. & Buffalo, E.A. Oscillatory activity in the monkey hippocampus during visual exploration and memory formation. *Proc Natl Acad Sci U S A* **110**, 13144-13149 (2013).

33. Dworkin, J.D. *et al.* The extent and drivers of gender imbalance in neuroscience reference lists. *bioRxiv* (2020).
34. Maliniak, D., Powers, R. & Walter, B.F. The gender citation gap in international relations. *International Organization* **67**, 889-922 (2013).
35. Caplar, N., Tacchella, S. & Birrer, S. Quantitative evaluation of gender bias in astronomical publications from citation counts. *Nature Astronomy* **1**, 0141 (2017).
36. Zhou, D., Cornblath, E.J., Stiso, J., Teich, E.G. & Dworkin, J.D. (2020).

Supp Fig 1

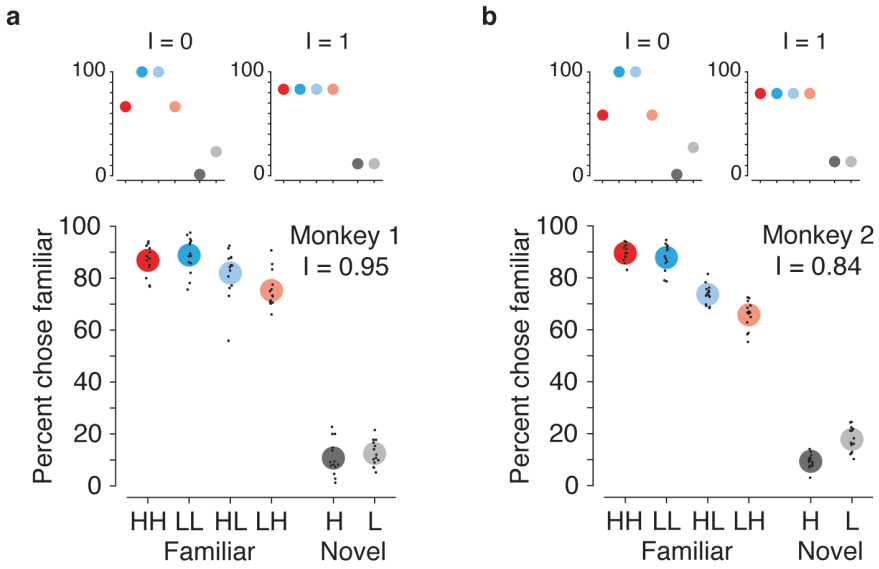

Supp. Fig. 1. *Behavioral performance patterns for individual monkeys.* **(a-b)** Figure 1c replotted for two animals. Small black dots indicate average performance for an individual session and large colored dots indicate the average performance across sessions (14 sessions per animal). The contrast invariance reflected in each behavioral pattern (I) is labeled in each plot. Insets correspond to behavioral patterns with maximal (I = 0) and minimal (I = 1) contrast confusion, matched for overall performance.

Supp Fig 2

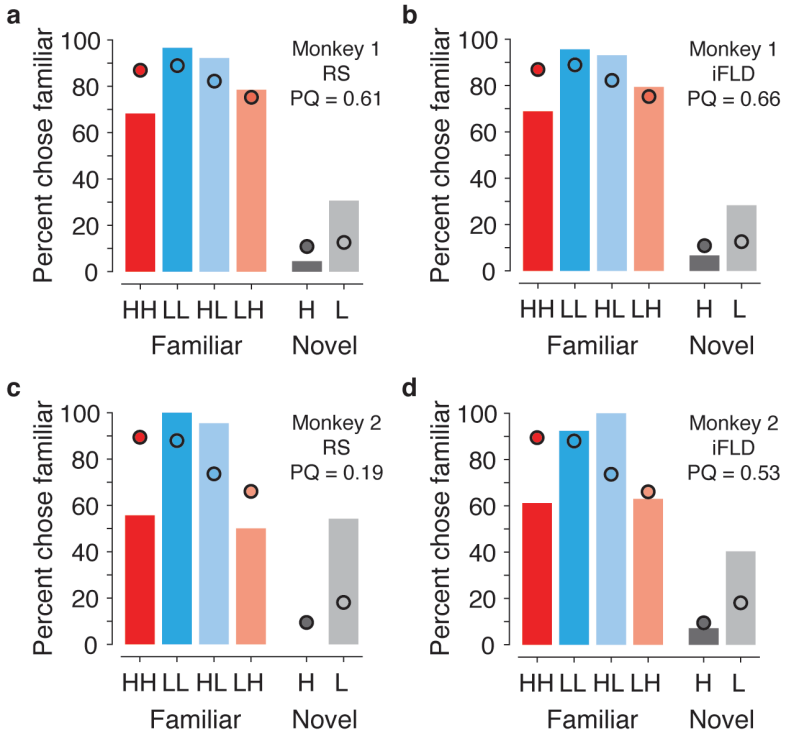

Supp. Fig. 2. *Classic linear decoders fail to map IT neural responses to behavior for each monkey.* **(a, c)** Fig 2a replotted for each animal. **(b, d)** Fig 2b replotted for each animal. In all panels, dots indicate the actual behavioral patterns and bars indicate the neural predictions of behavior for each type of linear decoder. Prediction quality (PQ) is indicated for each case.

Supp Fig 3

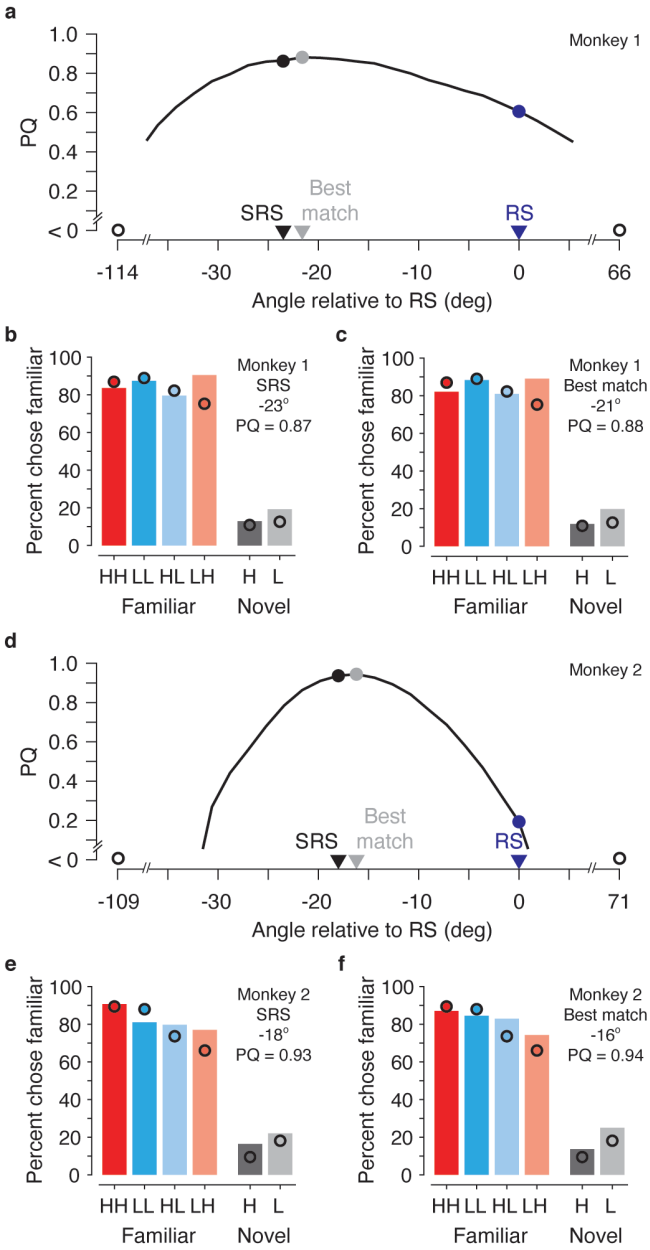

Supp. Fig. 3. *Neural predictions of behavior for a family of weighted linear decoders that include SRS, plotted for each monkey.* **(a, d)** Fig 3b, plotted for each animal: prediction quality (PQ) for the family of linear decoders that lie on the plane spanned by RS and contrast axis (Fig 3a). Markers correspond to SRS (black), RS (blue), and the linear decoder with largest PQ (grey). **(b, e)** Fig 3c, plotted for each animal: the alignment of the actual behavioral pattern and the SRS prediction **(c, f)** Fig 3d, plotted for each animal: the alignment of the actual behavioral pattern and the decoder with the highest PQ on this plane. In b-f, dots indicate actual behavioral patterns and bars indicate the linearly decoded neural predictions of behavior. The decoder's direction relative to RS, and prediction quality (PQ) are labeled for each case.

Supp Fig 4

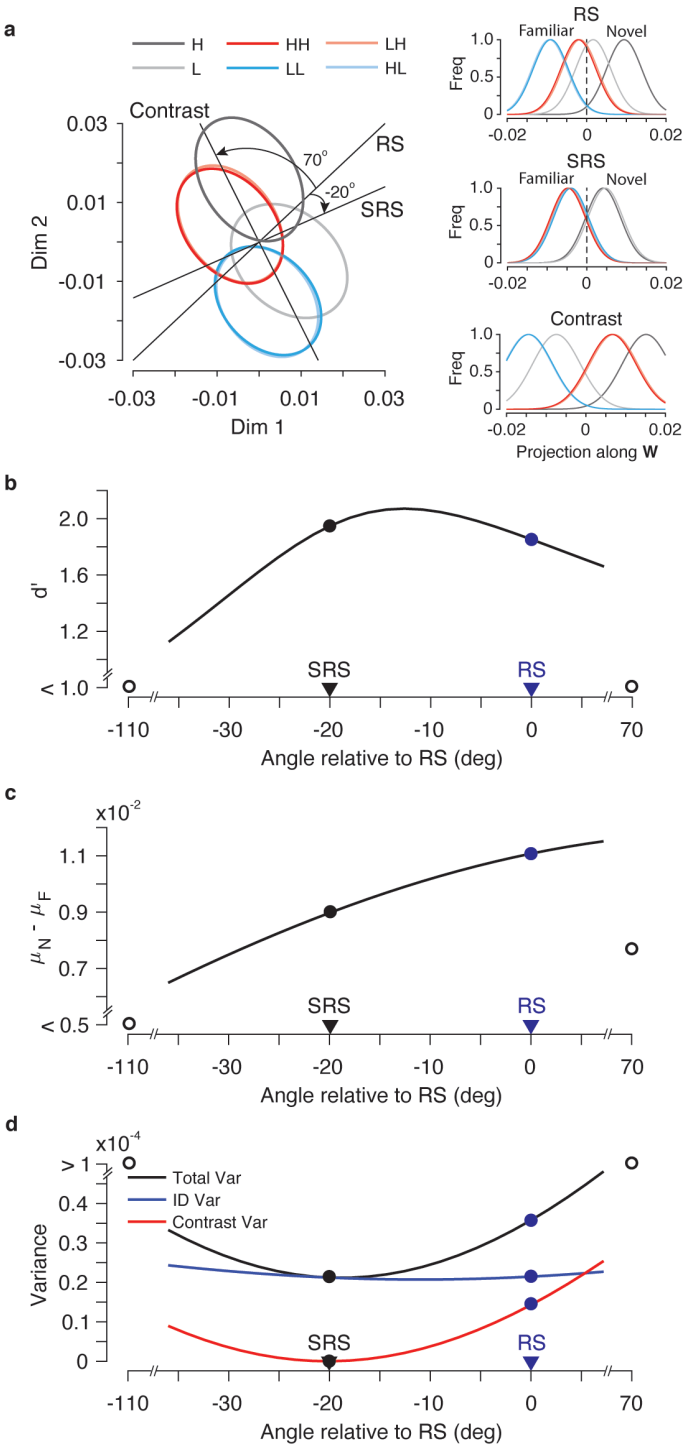

Supp. Fig. 4. *Synthetic data generated from the 4-parameter model recapitulates the actual data.* Simulations were performed for 650 units * 4K images (1K images/condition). All analyses were performed in the same manner as described for the physiological data. Plotted for the synthetic data **(a)** Fig. 3a **(b-d)** Fig. 4b-d.

Methods

Experiments were performed on two adult male rhesus macaque monkeys (*Macaca mulatta)* with implanted head posts and recording chambers. All procedures were performed in accordance with the guidelines of the University of Pennsylvania Institutional Animal Care and Use Committee.

The single-exposure, contrast-invariant visual memory task:

All behavioral training and testing were performed using standard operant conditioning (juice reward), head stabilization, and high-accuracy, infrared video eye tracking. Stimuli were presented on an LCD monitor with an 85 Hz refresh rate using customized software (http://mworks-project.org).

As an overview of the monkeys' task, each trial involved viewing one image for 500 ms, after which the monkeys indicated whether it was novel (never seen before) or familiar (seen exactly once prior) with an eye movement to one of two response targets. Images were never presented more than twice during the entire training and testing period of the experiment. Trials were initiated when the monkey fixated on a small red square (0.25°) on the center of a gray screen followed by a 200 ms delay before a 4° image appeared within a circular aperture. The monkeys needed to maintain fixation of the stimulus for 500 ms, at which time the red square turned green (the go cue) and the targets appeared. The monkeys then made a saccade to a target indicating whether the stimulus was novel or familiar, and correct responses were rewarded with juice. Targets were positioned 8° above or below the stimulus. The association between the target (up vs. down) and the report (novel vs. familiar) was swapped between the two animals.

The images used in these experiments collected via an automated procedure that gathered images from the internet. Images smaller than 96*96 pixels were not considered. Eligible images were cropped to be square and resized to 256*256 pixels. Duplicate images were removed. Colored images were converted to grayscale and were presented at two contrasts ("low (L)" and "high (H)") in all possible combinations as novel and familiar (novel-familiar = low-low (LL); high-high (HH); low-high (LH); high-low (HL)). Contrast modifications were applied in a manner that did not adjust image luminance (L_v), the mean pixel intensity. Images with L_v outside the range 0.25 – 0.75 were excluded. The computation of contrast began by first computing the median of the pixel intensities that fell above and below L_v, $L_{v\text{-hi}}$ and $L_{v\text{-lo}}$. The native contrast for each image C_{native} was computed as:

$$C_{native} = (L_{v\text{-hi}} - L_v) + (L_v - L_{v\text{-lo}})$$

Each image was manipulated to produce a high contrast version (C_{hi} = 0.4) and low contrast version (C_{lo} = 0.2) via a procedure that maintained L_v for each image. Adjustments to contrast involved: 1) subtracting the mean pixel value, 2) rescaling the residual pixel values all by the same amount, and 3) adding back the mean. When the procedure resulted in the saturation of more than 10% of pixels beyond their maximal value (black and white), that image was excluded.

Trial locations for novel images and their repeats were presented with a uniform distribution of the subset of n-back used in the experiment. The n-back distribution was adjusted for each monkey based on training history to approximately equate overall performance between the two animals: n-back = 1, 4, 16, and 32 for monkey 1, and n-back = 1, 2, 4, and 8 for monkey 2. The specific random sequence of images presented during each session was generated offline before the start of the session. Uniform n-back distributions were achieved by constructing a

sequence slightly longer than what was anticipated to be needed for the session, and by iteratively populating the sequence with novel images and their repeats at positions selected randomly from all the possibilities that remained unfilled. Because the longest n-back values (8 or 32) were the most difficult to fill, a fixed number of those were inserted first. In the relatively rare cases that the algorithm did not converge, it was restarted. The result was a partially populated sequence in which 83% of the trials were occupied. Next, the remaining 17% of trials were examined to determine whether they could be filled with novel/familiar pairs from the list of possible n-back options. The very small number of trials that remained after all possibilities had been extinguished (e.g. a 3-back scenario) were filled with 'off n-back' novel/familiar image pairs and these trials were disregarded in later analyses.

The monkeys' behavioral patterns were computed for each condition after collapsing across n-back. The degree of contrast invariance reflected in each monkey's session-averaged behavioral patterns was computed as the mean of contrast invariance computed for the novel and familiar memory conditions separately. Within each memory condition M, contrast invariance (I) of the behavioral pattern X in either memory condition was defined by:

$$\mathrm{I} = 1 - \frac{\mathrm{Var(X)}}{\mathrm{Var}(\mathrm{X}_{max})} \quad (1)$$

Where, $\mathrm{Var(X)}$ is the variance of pattern X, and $\mathrm{Var}(\mathrm{X}_{max})$ is the maximum possible variance associated with contrast in memory condition M given monkeys' overall performance in the same memory condition M. For example, the X_{max} for an overall performance across the familiar conditions of 85% would correspond to 70%, 100%, 100% and 70% for HH, LL, HL and LH, respectively.

Neural recording:

The activity of neurons in IT was recorded via a single recording chamber in each monkey. Chamber placement was guided by anatomical magnetic resonance images in both monkeys. The region of IT recorded was located on the ventral surface of the brain, over an area that spanned 5 mm lateral to the anterior middle temporal sulcus and 14-17 mm anterior to the ear canals. Recording sessions began after the monkeys were fully trained on the task and behavioral performance had plateaued. The depth and extent of IT was mapped within the recording chamber in a previous experiment [1]. Combined recording and behavioral training sessions happened 2-5 times per week across a span of 4 weeks (monkey 1) and 6 weeks (monkey 2). Neural activity was recorded with 24-channel U-probes (Plexon, Inc.) with linearly arranged recording sites spaced with 100 μm intervals. Continuous, wideband neural signals were amplified, digitized at 40 kHz and stored using the Grapevine Data Acquisition System (Ripple, Inc.). Spike sorting was done manually offline (Plexon Offline Sorter). At least one candidate unit was identified on each recording channel, and 2-3 units were occasionally identified on the same channel. Spike sorting was performed blind to any experimental conditions to avoid bias. A multi-channel recording session was included in the analysis if: (1) the recording session was stable, quantified as the grand mean firing rate across channels changing less than 3-fold across the session; (2) over 50% of neurons were visually responsive (a loose criterion based on our previous experience in IT), assessed by a visual inspection of the rasters; and (3) the number of successfully completed novel/familiar pairs of trials exceeded 100. In monkey 1, 19 sessions were recorded and five were removed (one based on criterion 1 and four based on criterion 3). In monkey 2, 15 sessions were recorded and one was removed (based on criterion 1). The resulting data set included 14 sessions for monkey 1 (n = 427

candidate units), and 14 sessions for monkey 2 (n = 429 candidate units). The sample size (number of successful sessions recorded) was chosen based on our previous work [1].

The data reported here correspond to the subset of images for which the monkeys' behavioral reports were recorded for both novel and familiar presentations (e.g. trials in which the monkeys did not prematurely break fixation during either the novel or the familiar presentation of an image). Accurate estimate of population response magnitude requires many hundreds of units, and when too few units are included, magnitude estimates are dominated by the stimulus selectivity of the sampled units. To perform our analyses, we thus concatenated units across sessions to create larger pseudopopulations. When creating these pseudopopulations, we aligned data across sessions in a manner that preserved whether the trials were presented as novel or familiar and their experimental contrast condition. To prevent artificial correlations from influencing our results, analyses were performed after re-randomizing the responses within each condition for each unit to create many pseudopopulations. To deal with varying data sizes across sessions, the number of images included in the analysis was selected to balance incorporating data of equal sizes across sessions with not needlessly discarding data. NaNs were used as place holders for the more limited sessions in which data did not exist. The resulting pseudopopulations consisted of the responses to 180 images presented as both novel and familiar (i.e. 45 images per condition: HH, LL, HL and LH). Spikes were counted in a temporal window over the range 100-500 ms following stimulus onset.

Linear population decoders:

For all decoders, the population response was quantified as the vector $\mathbf{x}$ containing spike counts on a given trial. To ensure that the decoder did not erroneously rely on visual selectivity, the decoder was trained on balanced pairs of novel/familiar trials in which monkeys viewed the same image (regardless of behavioral outcome or experimental contrast condition).

Cross-validated training and testing:

We applied the same, iterative cross-validated linear decoding procedure for each decoder. On each iteration of the resampling procedure, the responses for each unit were randomly shuffled within each experimental condition to ensure that artificial correlations (e.g. between the neurons recorded in different sessions) were removed. Each iteration also involved setting aside the responses to one randomly selected image within each contrast condition (presented as both novel and familiar, for 8 trials in total) for testing classifier performance. The remaining trials were used to train one of the linear decoders to distinguish novel versus familiar images invariant to contrast, where the novel and familiar classes included the data corresponding to all n-backs and all trial outcomes. A neural prediction of the proportion of trials on which "familiar" would be reported was computed as the proportion of each distribution that took on a value less than the criterion. Finally, the predicted response pattern was rescaled by a rescaling parameter (see below) as a proxy for adjusting the population size to consider.

All decoders in this study took the general form of linear discriminators. The class (novel/familiar) of a population response vector, $\mathbf{x}$ was determined by the sign of:

$$f(\mathbf{x}) = \mathbf{w}.\mathbf{x} - b \tag{2}$$

where **w** is the weight vector in the N-dimensional IT neural space (and N is the number of units), and *b* is decision criterion, given by:

$$b = \frac{1}{2}\mathbf{w}.(\boldsymbol{\mu}_N + \boldsymbol{\mu}_F) \tag{3}$$

Here $\boldsymbol{\mu}_N$ and $\boldsymbol{\mu}_F$ are the mean population response vectors across novel and familiar images in the training set, respectively. A population response vector $\mathbf{x}$ was classified as "novel" if $f(\mathbf{x}) > 0$, and "familiar" if $f(\mathbf{x}) < 0$.

Spike count classifier (associated with repetition suppression, RS):

Arguably the simplest classifier, the total spike decoder uses a homogeneous weight vector:

$$\mathbf{w}_{RS} = \mathbf{1} = (1, 1, \ldots, 1) \tag{4}$$

Fisher Linear Discriminant (iFLD):

The iFLD used in this study follows our previous implementation[1]. The Fisher Linear Discriminant (FLD) is defined as:

$$\mathbf{w}_{FLD} = \Sigma^{-\mathbf{1}}(\boldsymbol{\mu}_N - \boldsymbol{\mu}_F) \tag{5}$$

where Σ^{-1} is the inverse of the mean covariance matrix across novel and familiar conditions:

$$\Sigma = \frac{1}{2}(\Sigma_N + \Sigma_F) \tag{6}$$

The dimensionality of our neural populations is high enough that we do not have enough data to obtain reliable covariance estimates (we estimate the amount of data needed to estimate the off-diagonal entries is >10-fold what we collected in a single session). As such, we assume independence of the stimulus responses within conditions (i.e., we set the off-diagonal entries to zero). The resulting iFLD uses a weight for each unit that is proportional to its familiarity discriminability (d'):

$$\mathbf{w}_{iFLD} = \sum_{i=1}^{N} \mathbf{e_i} \left(\frac{\mu_N^{(i)} - \mu_F^{(i)}}{{\sigma_i}^2} \right) \tag{7}$$

where $\mathbf{e_i}$ is the unit vector along *i*-th dimension (*i*-th unit's response); N is the number of units; $\mu_N^{(i)}$ and $\mu_F^{(i)}$ are *i*-th unit's mean responses to novel and familiar images, respectively; and ${\sigma_i}^2$ is the *i*-th unit's average response variance across novel and familiar conditions:

$${\sigma_i}^2 = \frac{1}{2}\left({\sigma_N^{(i)}}^2 + {\sigma_F^{(i)}}^2\right) \tag{8}$$

Family of contrast-corrected linear decoders:

The family of contrast-corrected linear decoders are based on weight vectors that are rotated within the plane containing the RS decoder ($\mathbf{1}$) and a contrast decoder, $\mathbf{w_c}$:

$$\hat{\mathbf{w}}(\theta) = (\cos\theta - \cot\gamma \sin\theta)\hat{\mathbf{1}} + (\csc\gamma \ \sin\theta)\hat{\mathbf{w}}_{\boldsymbol{c}}\,; \quad \theta \in [\gamma - \pi, \gamma] \tag{9}$$

where, $\hat{\mathbf{w}}(\theta)$, $\hat{\mathbf{1}}$ and $\hat{\mathbf{w}}_{\boldsymbol{c}}$ are the unit vectors along the decoding axes, RS decoder, and contrast decoder, respectively. θ is the angle between the decoder axis ($\hat{\mathbf{w}}(\theta)$) and the RS axis ($\mathbf{1}$), and γ is the angle between the RS and contrast axes. The contrast weight vector $\mathbf{w_c}$ was defined as:

$$\mathbf{w_c} = (\boldsymbol{\mu}_H - \boldsymbol{\mu}_L) \tag{10}$$

Where $\boldsymbol{\mu}_H$ and $\boldsymbol{\mu}_L$ are the mean population response vectors across high and low contrast images in train set, respectively. This is a simple form of FLD that arises when the average covariance is a multiple of the identity, and is sometimes called a "prototype classifier". We define the SRS decoder as the axis which is orthogonal to contrast, i.e.

$$\theta_{SRS} = \gamma - \frac{\pi}{2} \tag{11}$$

Rescaling parameter and prediction quality (PQ):

Comparing IT population decoding performance with behavior depends on the neural population size under consideration, and there is no good way to choose this *a priori.* We thus applied a fitting approach for each decoder. After confirming that performance using all recorded units in our dataset fell below saturation, we simulated increases in population size by fitting a single rescaling parameter (α) to minimize the MSE between the neural predictions and actual behavioral patterns. We emphasize that while this adjustment changed the overall performance, it did not impact the shape of the predicted behavioral patterns. The minimization of MSE yields an analytical solution for α as:

$$\alpha = \frac{\sum_{i=1}^{6} \hat{y}_i y_i}{\sum_{i=1}^{6} {y_i}^2} \tag{12}$$

where $\hat{y}_i$ and y_i are the actual and neutrally predicted performance for condition i, respectively, and i corresponds to each of six conditions including HH, LL, HL, LH, H, and L. Next, to quantify the quality of the fit after rescaling the predicted pattern, we computed a measure of prediction quality (PQ):

$$\mathrm{PQ} = 1 - \frac{MSE}{MSE_{max}} \tag{13}$$

where *MSE* and MSE_{max} denote the mean square error of the rescaled predicted pattern and the pattern with maximum MSE that was matched in overall performance, respectively, i.e.

$$MSE = \frac{1}{6}\sum_{i=1}^{6} (\hat{y}_i - {y'}_i)^2 \tag{14}$$

and

$$MSE_{max} = \underset{\delta_i}{\operatorname{argmax}} \left(\frac{1}{6} \sum_{i=1}^{6} (\hat{y}_i - \delta_i)^2 \right) \tag{15}$$

$\hat{y}_i$ and y'_i are the actual and rescaled predicted performance for condition i, respectively, and i corresponds to each of six conditions including HH, LL, HL, LH, H, and L. δ_i could be either 1 (highest performance) or $2\bar{y} - 1$ (lowest possible performance given the overall performance) depending on which one is larger. $\bar{y}$ is the mean performance across all six conditions. The upper bound of PQ = 1 reflects a neural prediction that perfectly replicates the actual behavioral pattern. A PQ = 0 reflects the worst possible predicted behavioral pattern that was matched in overall performance. Negative PQ values reflect predicted behavioral patterns that could not be rescaled with α to match overall performance because one or more entries were pinned at saturation (e.g., as a consequence of extreme contrast modulation).

Covariance error ellipse:

Error ellipses (shown in Fig 3a, 5a, and Supp Fig 4a) were computed by first projecting the neural response vectors onto the non-orthogonal discriminant axes $\hat{\mathbf{1}}$ and $\hat{\mathbf{w}}_{\boldsymbol{c}}$, producing coordinates (u, v). These were transformed to orthogonal coordinates using a transformation matrix (derived from Eq. (9)):

$$\mathrm{R} = \begin{bmatrix} 1 & 0 \\ -\cot\gamma & \csc\gamma \end{bmatrix} \tag{16}$$

where γ is the angle between the two discriminant axes:

$$\gamma = \angle(\mathbf{w_1}, \mathbf{w_2}) = \operatorname{acos}(\mathbf{w_1} \cdot \mathbf{w_2}) \tag{17}$$

We then rotate this coordinate system in the plane by angle φ, using transformation matrix:

$$\mathrm{R}_{\varphi} = \begin{bmatrix} \cos\varphi & -\sin\varphi \\ \sin\varphi & \cos\varphi \end{bmatrix} \tag{18}$$

Combining Eq (16) and (18) gives an expression for the (x, y) coordinates of the projected neural responses:

$$\begin{bmatrix} x \\ y \end{bmatrix} = \begin{bmatrix} \cos\varphi & -\sin\varphi \\ \sin\varphi & \cos\varphi \end{bmatrix} \times \begin{bmatrix} 1 & 0 \\ -\cot\gamma & \csc\gamma \end{bmatrix} \times \begin{bmatrix} u \\ v \end{bmatrix} \tag{19}$$

For each condition, the covariance matrix of the transformed data was computed, and the eigenvectors of this matrix provide the major and minor axes of the associated ellipse. To determine the dimensions of the ellipse, we multiplied the square root of the eigenvalues by a scale factor equal to the square root value of the cumulative chi-square distribution function (CDF) for 2-degrees of freedom evaluated at 95%.

Decomposition of total variance into variance due to identity/trial variability and contrast:

For Figs 4, 5, and Supp Fig 4, we used the following equations to decompose the average variance across novel (N) and familiar (F) conditions, $\sigma_{avg}{}^2 = \frac{1}{2}(\sigma_N{}^2 + \sigma_F{}^2)$, into the variance due to image identity and trial variability (ID) and contrast (C):

$$\sigma_{avg}{}^2 = \frac{1}{2}(\sigma_{ID}{}^2 + \sigma_C{}^2)$$

Where:

$$\sigma_{\mathrm{ID}}{}^2 = \frac{1}{2}(\sigma_H{}^2 + \sigma_L{}^2) + \frac{1}{4}(\sigma_{HH}{}^2 + \sigma_{LL}{}^2 + \sigma_{HL}{}^2 + \sigma_{LH}{}^2)$$

$$\sigma_{\mathrm{C}}{}^2 = \frac{1}{2}[(\mu_H{}^2 - \mu_N{}^2) + (\mu_L{}^2 - \mu_N{}^2)] + \cdots \frac{1}{4}[(\mu_{HH}{}^2 - \mu_F{}^2) + (\mu_{LL}{}^2 - \mu_F{}^2) + (\mu_{HL}{}^2 - \mu_F{}^2) + (\mu_{LH}{}^2 - \mu_F{}^2)] \quad (20)$$

In each condition, σ and μ denote the standard deviation and mean of the corresponding distribution, respectively.

Fitting the four-parameter tuning model to each unit and synthesizing data:

In Figure 5, we assessed the population geometry in the limit of infinite samples by fitting a model to each unit that we recorded, and then using these models to synthesize population data. A 4-parameter model was used to describe the mean spike count response of each unit:

$$y(x; M, C) = A.m.c.\exp(-ax) \quad (21)$$

where x is stimulus rank, M is image memory condition (novel or familiar), C is image contrast (high or low), A is amplitude, m is memory modulation (set to 1 for novel images, and a fitted value for familiar images), c is contrast modulation (set to 1 for high contrast images, and fitted value for low contrast), and a controls stimulus selectivity.

We estimated each unit's tuning curve parameters by maximizing the likelihood (MLE) of observing the spike count data from 100 ms to 500 ms relative to stimulus onset using the techniques introduced in ref. [2]. If $\{v_1, v_2, \ldots, v_n\}$ is the spike count data for a unit in all six conditions (n trials in total), the log-likelihood of observing the data is given by:

$$\log \mathcal{L}(v|\, A, \alpha, m, c) = \sum_{i=1}^{n} \log\big(P(v_i|A, \alpha, m, c)\big) \quad (22)$$

where

$$P(v|A,\alpha,m,c)=\begin{cases}1+\frac{1}{a}\sum_{k=1}^{\infty}\frac{(-1)^k {A_X}^k}{k.k!}\left(1-e^{-ka}\right) & ;v=0\\ \frac{1}{a.v}\sum_{k=0}^{v-1}\frac{{A_X}^k}{k!}\left(e^{-(ka+A_X e^{-\alpha})}-e^{-A_X}\right); v\neq 0\end{cases} \tag{23}$$

and

$$A_X=\begin{cases}A & ;X\text{: H}\\ c.A & ;\ X\text{: }L\\ m.A & ;X\text{: }HH\text{, or }LH\\ m.c.A & ;X\text{: }LL\text{, or }HL\end{cases} \tag{24}$$

We estimated four tuning parameters of the unit by maximizing (22) with respect to the parameters A, a, m, and c.

Goodness of fit was assessed by comparing the actual and predicted grand mean spike counts, and only accepting units whose predicted grand mean spike counts fell in the range 0.83-1.2x of the actual values. Of 856 units, 661 units fulfilled this criterion.

Finally, we used the tuning parameters for each unit to synthesize the responses to 1000 images per condition. For each unit, we sampled x in Equation 21 as 1000 draws from a uniform distribution between 0 and 1 and used those values to compute spike count rates, which were converted to spike counts by drawing from a Poisson process.

1. Meyer, T. & Rust, N.C. Single-exposure visual memory judgments are reflected in inferotemporal cortex. *eLife* **7**, e32259 (2018).
2. Goris, R.L., Movshon, J.A. & Simoncelli, E.P. Partitioning neuronal variability. *Nat Neurosci* **17**, 858-865 (2014).